Supporting Information

Combining crossed-lamellar structure and nacre-like nanoparticulate structure in conch shells for enhanced mechanical properties

Mingshu Jin[a,b,#], Ping Yuan[c,#], Luyao Yi[b*], Zhuanfei Liu[b], Zhengyi Fu[b] and Zhaoyong Zou[a,b*]

[a]*Hubei Longzhong Laboratory, Wuhan University of Technology Xiangyang Demonstration Zone, Xiangyang 441000, China;*
[b]*State Key Laboratory of Advanced Technology for Materials Synthesis and Processing, Wuhan University of Technology, Wuhan 430070, China;*
[c]*School of Materials Science and Engineering, Wuhan University of Technology, Wuhan 430070, China;*
[#]These authors contributed equally to this work.
[*]Corresponding authors.

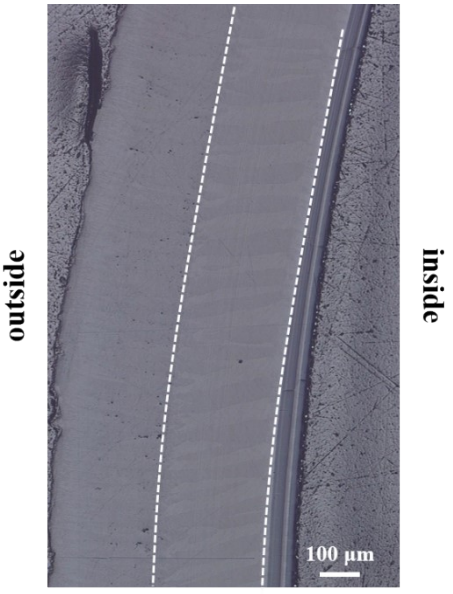

Supplementary Figure 1 Optical photo of coaxial drop mode ultra depth of field after three-layer region polishing, it could be clearly seen that the structure of the three-layer was different.

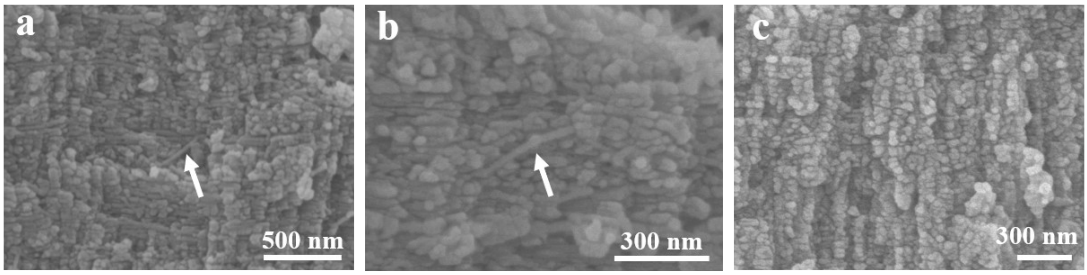

Supplementary Figure 2 (a-c) Enlarged SEM images of nanoparticles and organic networks and the white arrows represented the organic networks.

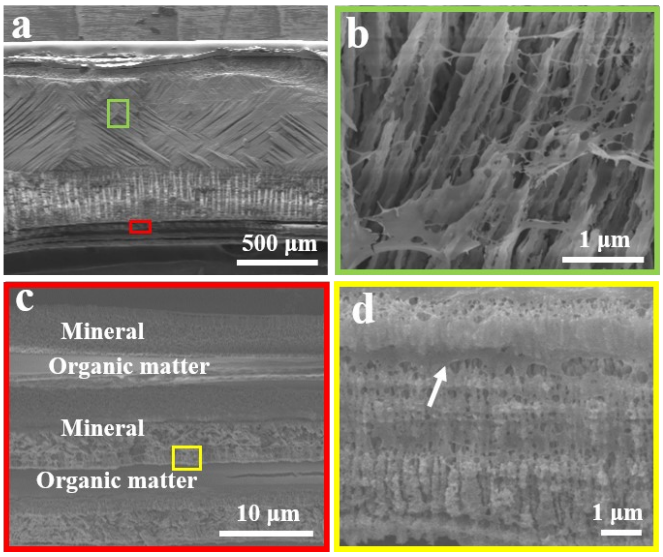

Supplementary Figure 3 SEM images of the three-layer region of shells after demineralization. (a) Overall view of the three-layer region after demineralization. (b) SEM image of the crossed-lamellar structure after demineralization. (c) SEM image of the nanoparticle layer structure after demineralization, white arrows refer to organic matter. (d) Organic matter between nanoparticles.

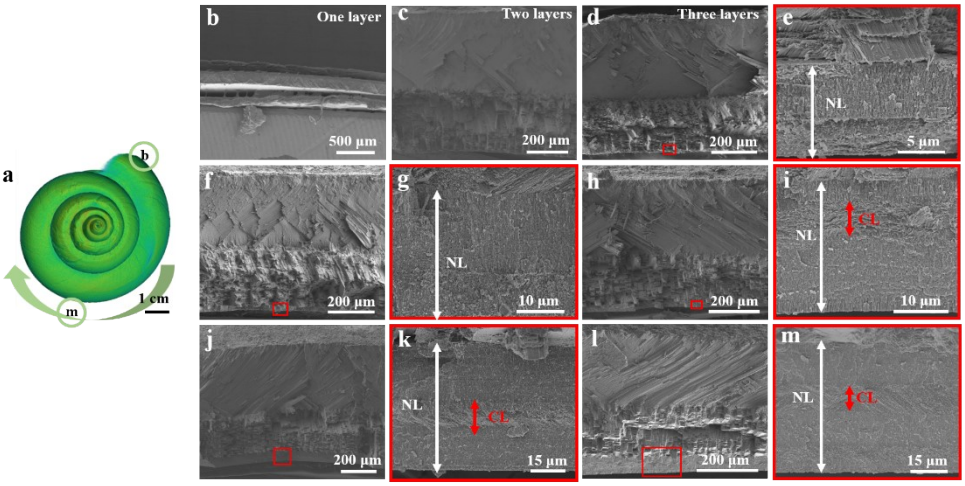

Supplementary Figure 4 Microstructure of different parts of conch shell in transverse direction. (a) Top view of conch shell. (b) SEM image of outer lip. (c)-(m) SEM images of different parts of conch shell following the direction of the arrows in (a). (e), (g), (i), (k), (m) Enlarged SEM of (d), (f), (h), (j), (l) respectively.

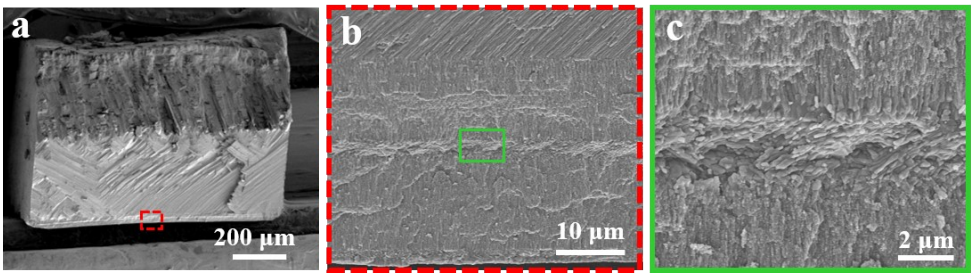

Supplementary Figure 5 SEM images of higher resolution micro-CT (700 nm/voxel). (a) Sectional view of the CT sample. (b) Enlarged SEM image of (a). (c) Enlarged SEM image of (b), showing different forms of minerals.

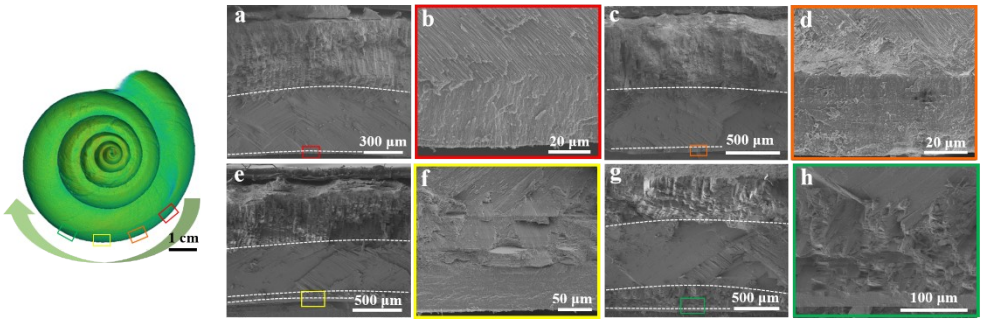

Supplementary Figure 6 (a)-(h) Microstructure of different parts of conch shell, which showed the four-layer structure, with three crossed-lamellar structure and one nanoparticle layer. (b), (d), (f), (h) Enlarged SEM of (a), (c), (e), (g) respectively.

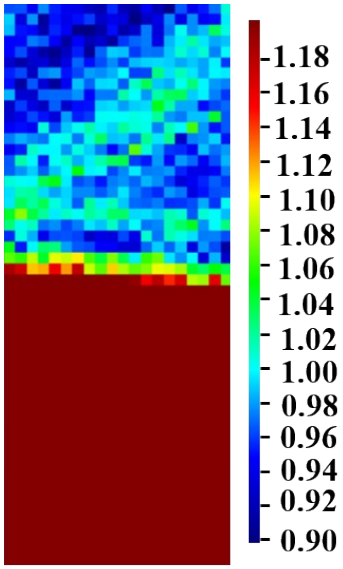

Supplementary Figure 7 Raman maps acquired from the region indicated in e showing the changes of the ratio between the intensity of peak at 150 cm^{-1} and 204 cm^{-1}, showing the mineral orientation of the cross-lamellar structure.

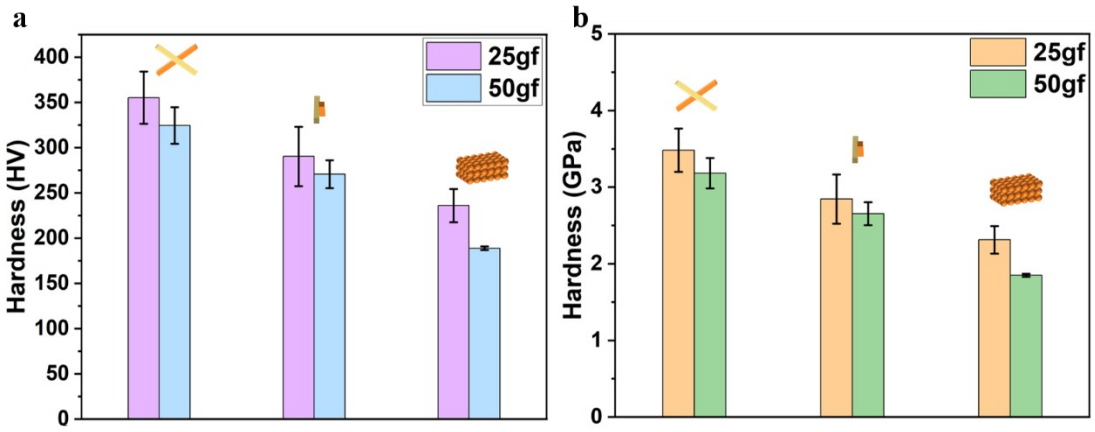

Supplementary Figure 8 (a) and (b) Vickers hardness values for different microstructures. The unit of (a) was HV, the unit of (b) was GPa**.**

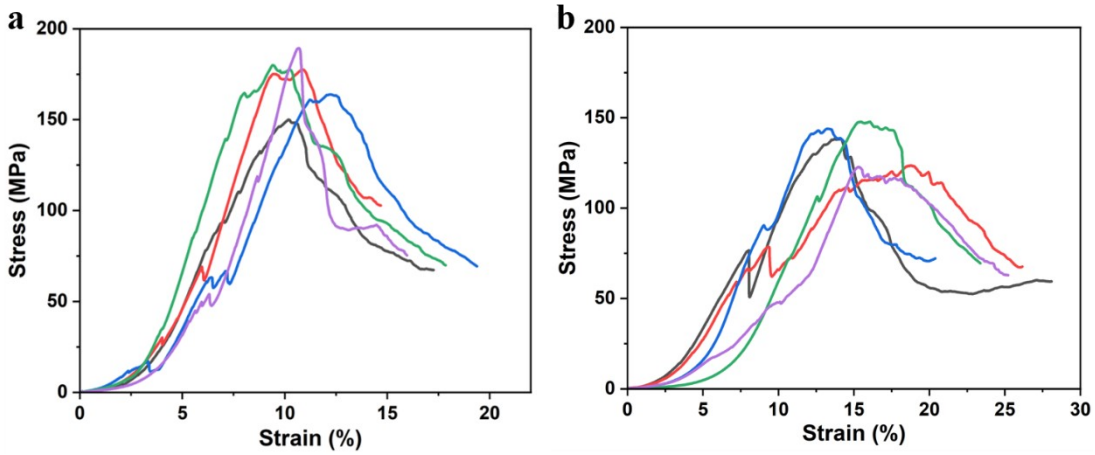

Supplementary Figure 9 (a) Compression stress-strain curves in the three-layer region. (b) Compression stress-strain curves in the two-layer region. The compressive strength of the three-layer region was higher than that of the two-layer region.

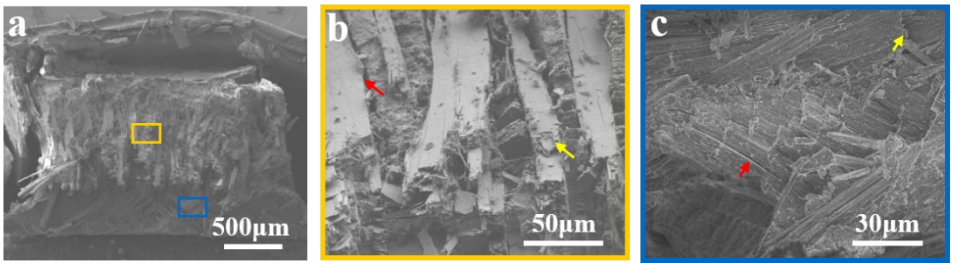

Supplementary Figure 10 (a) SEM image of the compressed sample with failure in the two-layer region of the conch shell. (b) Magnification of the yellow box in (a), it shows the crack propagation when the crossed-lamellar structure was compressed. (c) Magnification of the blue box in (a), red arrows represent first-order lamellae interface failure and yellow arrows represent second-order lamellae interface failure.

Supplementary Movie 1 Micro-CT data and visualization of the whole conch shell. Voxel size = 8 μm.

Supplementary Movie 2 High resolution Micro-CT data and visualization of the dorsal region of conch shell. Voxel size = 700 nm.